The Seventh Asian-Pacific Symposium on Structural Reliability and Its Applications (APSSRA2020)
October 4–7 2020, Tokyo, Japan
T. Takada, I. Yoshida & T. Itoi (editors)

Time-Dependent System Reliability Analysis of Slopes Under Rainfall Infiltration Using HLRF Algorithm

Wenwang Liao[1], and Jian Ji[2*]

1 Ph.D. Candidate, School of Civil and Transportation Engineering, Hohai University, 1 Xikang Road, Nanjing 210098, China. wwliao@hhu.edu.cn
2* Professor, School of Civil and Transportation Engineering, Hohai University, 1 Xikang Road, Nanjing 210098, China. JI0003AN@e.ntu.edu.sg

Abstract: The rainfall-induced earth slope stability is time dependent as a result of the infiltration process. In order to cater the consideration of uncertain parameters, we conduct a time-dependent reliability analysis of the rainfall-induced slope stability, which incorporates discretizing the time-dependent stochastic process, assigning instantaneous limit state functions at discrete time instants, and calculating the time-dependent reliability within the forecast time as a series system reliability considering all instantaneous limit state functions. We adopt a simplified HLRF (Hasofer-Lind-Rackwitz-Fiessler) algorithm to calculate the first-order reliability indices. At last, we make a case study of an earth slope under intensive rainfall conditions using the proposed method.

Keywords: Time-dependent failure, System reliability, FORM, Rainfall, Slope stability

1. Introduction

Due to the influence of geological processes, environmental conditions and human factors, slope instability and landslides have become a common engineering disaster and attracted worldwide research interests (Li et al., 2015) (Y. Zhang et al., 2018). The slope stability analysis is a complex system problem, which is greatly influenced by the uncertainty of load, spatial variability of soil parameters and calculation models (Baecher & Christian, 2003). To ensure that the structure system can work efficiently, the resistance R of the system must be bigger than the load F during the servicing period. The limit state function (*LSF*) can be expressed as $G = R - F$; when $G < 0$, the system will be in a failure condition, and when it suffers a failure condition for a sufficiently long time, the structure will be destroyed (Liu & Der Kiureghian, 1991).

During the servicing period, some physical properties of the structure may deteriorate with time and the resistance of the structure is reduced. Moreover, the load fluctuations will also influence the stability of the system. With the reduction of the resistance and the increase of the load, the system has an increasing probability of falling into the failure domain. Reliability-based optimization (RBO) is a methodology that determines the best design solution according to certain predefined design criteria while explicitly considering the effects of uncertainty (Valdebenito & Schuëller, 2010). The purpose of the time-dependent design and analysis of a structure system is to make the changes of the resistance and the load clearer for engineering designers, and some efficient prevention measures will be proposed before the failure of the structure system.

In this study, we calculate the time-dependent reliability index using a variant of HLRF-x algorithm that can be directly used in x-space without any intermediate mathematical manipulations; a simplified procedure with numerical differentiation analysis in x-space is used for conducting system reliability analysis of the rainfall-induced slope stability via Python platform.

2. Concept of FORM using HLRF-x algorithm

The classical FORM needs complicated mathematical manipulation to transform original correlated basic random variables $\mathbf{x}$ (x-space, non-Gaussian type) into correlated standardized normal variables $\mathbf{n}$ (n-space), and further into uncorrelated standardized normal variables $\mathbf{u}$ (u-space), and the Hasofer-Lind index β is defined as (Hasofer & Lind, 1974):

$$\beta = \sqrt{\mathbf{u}^{*T}\mathbf{u}^{*}} \tag{1}$$

where the vector $\mathbf{u}^*$ is the design point, denoting the point on the limit state surface (*LSS*) $g(\mathbf{u}) = 0$ closest to the origin of u-space. An iterative algorithm to search for $\mathbf{u}^*$ is well explained by (Ang & Tang, 1975; Mahadevan & Haldar, 2000; R Rackwitz, 1976), and an alternative formulation of β in x-space or n-space is presented by (Bak K Low & Tang, 2004; B. K. Low & Tang, 2007):

$$\beta = \sqrt{\mathbf{n}^{*T}\,\mathbf{R}^{-1}\mathbf{n}^{*}} = \sqrt{\left(\frac{x_i^{*}-u_i^{N}}{\sigma_i^{N}}\right)^{T}\mathbf{R}^{-1}\left(\frac{x_i^{*}-u_i^{N}}{\sigma_i^{N}}\right)} \tag{2}$$

where x_i^* is the design point value of the ith variable evaluated in x-space, μ_i^N and σ_i^N are equivalent normal mean and standard deviation of the ith variable, respectively, $\mathbf{R}$ is the correlation matrix, and $\mathbf{n}^*$ is the design point evaluated in n-space. Parameters μ_i^N and σ_i^N can be calculated by the Rackwitz–Fiessler transformation (Rüdiger Rackwitz & Flessler, 1978). When *LSF* is explicit, x_i^* and β can be easily computed using a constrained optimization approach using the Low and Tang approaches (Bak K Low & Tang, 2004; B. K. Low & Tang, 2007); when *LSF* is implicit, the constrained optimization approach needs to be used in combination with response surface method (*RSM*) for the *LSF* approximation(J. Ji & Low, 2012). On the other hand, it is more desirable to carry out reliability analysis with no requirement for approximating the actual *LSF*. In this

regard, the HL–RF recursive algorithm for FORM (Liu & Der Kiureghian, 1991; Mahadevan & Haldar, 2000; Rüdiger Rackwitz & Flessler, 1978) can be used as an alternative. It first linearizes the *LSF* at each iteration point instead of searching for design point by subjecting to an explicit *LSF*, the recursive algorithm uses the derivatives to find the next iteration point, such that

$$\mathbf{u}_{k+1} = \frac{1}{\left|\nabla g(\mathbf{u}_k)\right|^2}\left[\nabla g(\mathbf{u}_k)^T \mathbf{u}_k - g(\mathbf{u}_k)\right]\nabla g(\mathbf{u}_k) \tag{3}$$

where $\mathbf{u}_k$ is the kth iteration point in u-space and $g(\mathbf{u}_k)$ and $\nabla g(\mathbf{u}_k)$ are the performance function and gradient vectors of the performance function evaluated at $\mathbf{u}_k$, respectively. In general, the gradient vector is not constant when non-linear *LSF* is involved. As a result, the iterative evaluation of Eq (3) is needed to obtain the design point $\mathbf{u}^*$. (Jian Ji & Kodikara, 2015) reformulates the recursive algorithm completely in x-space. The basic random variables $\mathbf{x}$ has a correlation matrix $\mathbf{R}$ which is still unchanged when $\mathbf{x}$ transforms into correlated standardized normal variables $\mathbf{n}$, using Cholesky decomposition to transform correlated standardized normal variables $\mathbf{n}$ into uncorrelated standardized normal variables $\mathbf{u}$, such that

$$\mathbf{R} = \mathbf{L}\mathbf{L}^{\mathrm{T}} \tag{4}$$

$$\mathbf{n} = \mathbf{L}\mathbf{u} \tag{5}$$

where $\mathbf{L}$ is a lower triangular matrix decomposed by correlation matrix $\mathbf{R}$. the gradient vector of performance function can be translated from u-space to n-space and x-space, respectively.

$$\nabla g(\mathbf{u}_k) = \mathbf{L}^{\mathrm{T}} \nabla g(\mathbf{n}_k) = \mathbf{L}^{\mathrm{T}}\left[\boldsymbol{\sigma}_k^N\right]\nabla g(\mathbf{x}_k) \tag{6}$$

where the diagonal matrix $[\boldsymbol{\sigma}_k^N]$ consists of the equivalent normal standard deviation $\sigma_{k,i}^N$ of the ith random variable evaluated at $\mathbf{x}_k$.

Multiplying $\mathbf{L}$ to both sides of Eq (3), and using Eq (6), the HLRF recursive algorithm is reformulated to be (Jian Ji & Kodikara, 2015; Jian Ji et al., 2019):

$$\mathbf{n}_{k+1} = \frac{1}{\nabla g(\mathbf{n}_k)^T \mathbf{R} \nabla g(\mathbf{n}_k)}\left[\nabla g(\mathbf{n}_k)^T \mathbf{n}_k - g(\mathbf{n}_k)\right]\mathbf{R}\nabla g(\mathbf{n}_k) \tag{7}$$

$$\left[\frac{\mathbf{x}_{k+1} - \boldsymbol{\mu}_{k+1}^N}{\boldsymbol{\sigma}_{k+1}^N}\right] = \frac{1}{\nabla g(\mathbf{x}_k)^T \mathbf{T}_{\mathbf{k}} \nabla g(\mathbf{x}_k)} \bullet \left[\nabla g(\mathbf{x}_k)^T \left(\mathbf{x}_k - \boldsymbol{\mu}_k^N\right) - g(\mathbf{x}_k)\right]\mathbf{R}\left[\boldsymbol{\sigma}_k^N\right]\nabla g(\mathbf{x}_k) \tag{8}$$

where $\mathbf{T}_k = [\sigma_k^N]^T\mathbf{R}[\sigma_k^N]$ is a transformation matrix.
Because the iterative procedure is used to find the design point, it is appropriate to suppose $\mu_{k+1}^N \approx \mu_k^N$ and $\sigma_{k+1}^N \approx \sigma_k^N$, the right hand side is evaluated at $\mathbf{x}_k$. As such, Eq (3) can be re-written as

$$\mathbf{x}_{k+1} = \boldsymbol{\mu}_k^N + \frac{1}{\nabla g(\mathbf{x}_k)^T \mathbf{T}_k \nabla g(\mathbf{x}_k)} \times\left[\nabla g(\mathbf{x}_k)^T \left(\mathbf{x}_k - \boldsymbol{\mu}_k^N\right) - g(\mathbf{x}_k)\right]\mathbf{T}_k \nabla g(\mathbf{x}_k) \tag{9}$$

Similarly, the gradient vector may not be constant in x-space; hence, the proposed HLRF-x algorithm in Eq (9) requires the computation of the gradient vector of *LSF* at each iteration point. When the *LSF* is implicit, the gradient vector is commonly estimated by the partial numerical differentiation method. After obtaining the design point $\mathbf{x}^*$, the reliability index can be calculated by Eq (2), and the failure probability P_f is then approximated by:

$$p_f = \Phi(-\boldsymbol{\beta}) \tag{10}$$

where $\Phi(\cdot)$ = standard normal cumulative distribution function.

The *LSF* in different space can be approximated by:

$$g(\mathbf{u}^*) = \boldsymbol{\beta} - \boldsymbol{\alpha}^T\mathbf{u}^* = g(\mathbf{n}^*) = \boldsymbol{\beta} - \boldsymbol{\alpha}^T\mathbf{L}^{-1}\mathbf{n}^* = g(\mathbf{x}^*) = \boldsymbol{\beta} - \boldsymbol{\alpha}^T\mathbf{L}^{-1}\left(\frac{x_i^* - \boldsymbol{\mu}_i^N}{\boldsymbol{\sigma}_i^N}\right) = 0 \tag{11}$$

$$\boldsymbol{\alpha} = \frac{\mathbf{u}^*}{\boldsymbol{\beta}} = \frac{\mathbf{L}^{-1}\mathbf{n}^*}{\boldsymbol{\beta}} = \frac{\mathbf{L}^{-1}}{\boldsymbol{\beta}}\left(\frac{x_i^* - \boldsymbol{\mu}_i^N}{\boldsymbol{\sigma}_i^N}\right) \tag{12}$$

where $\boldsymbol{\alpha}$ is a unit vector normal pointing toward the failure domain.

3. Time-dependent system reliability

Consider that a time-dependent reliability problem is defined by the response limit state function as $G(t) = g(\mathbf{X}, \mathbf{Y}(t))$, where t denotes the time; $\mathbf{X} = [X_1, X_2, \ldots, X_n]$ is n-dimensional time-independent random variable vector; $\mathbf{Y}(t)=[Y_1(t), Y_2(t), \ldots, Y_m(t)]$ represents m-dimensional input random processes as a function of t. $G(t)\leq 0$ indicates the instantaneous failure at time t, and safety otherwise. The failure probability over the forecast time period $[0, T]$ is expressed by $P(0, T) = \Pr(G(\tau)\leq 0, \exists\, \tau\, [0, T])$, where $\Pr(\bullet)$ denotes the probability; T is the forecast time.

System random processes, $\mathbf{Y}(t)$, are uniformly discretized within the time period $[0, T]$ at finite numbers of N time instants. Let $g(x, y(\tau_k))$ (k=1, 2, …, N) denote the response limit state function at the discrete time instant τ_k ($0 \leq \tau_k \leq T$), where x and $y(\tau_k)$ represent the values of $\mathbf{X}$ and $\mathbf{Y}(\tau_k)$ (k=1, 2, …, N), respectively. The response functions $g(x, y(\tau_k))$ and $g(x, y(\tau_l))$ at different time instants, τ_k and τ_l (k, l=1, 2, …, N; $k\neq l$), are correlated due to the common variable vector of $\mathbf{X}$ and statistical dependence of random processes $\mathbf{Y}(\tau_k)$ and $\mathbf{Y}(\tau_l)$ (k, l=1, 2, …, N; $k\neq l$). Let the matrix $\mathbf{R}_{LSF}$ represents the correlation matrix of the limit state functions at different time, after getting different design point in different time instants, the correlations matrix $\mathbf{R}_{LSF}$ of the safety margins at each time instants must be evaluated for estimating the system reliability (Madsen et al., 2006; Zhou et al., 2017), such that:

$$\boldsymbol{\beta_\tau}=\sqrt{\left(\frac{x_{\tau i}^{*}-u_{\tau i}^{N}}{\sigma_{\tau i}^{N}}\right)^{T}\mathbf{R}_{\tau\tau}^{-1}\left(\frac{x_{\tau i}^{*}-u_{\tau i}^{N}}{\sigma_{\tau i}^{N}}\right)} \tag{13}$$

$$\rho_{kl}=\rho_{lk}=\boldsymbol{\alpha}_{\tau k}^{T}\boldsymbol{\alpha}_{\tau l}=\left[\frac{\mathbf{L}_k^{-1}}{\beta(\tau_k)}\left(\frac{x_{ki}^{*}-\mu_{ki}^{N}}{\sigma_{ki}^{N}}\right)\right]^{T}\times\frac{\mathbf{L}_l^{-1}}{\beta(\tau_l)}\left(\frac{x_{li}^{*}-\mu_{li}^{N}}{\sigma_{li}^{N}}\right) \tag{14}$$

where ρ_{kl} is one of the elements in $\mathbf{R}_{LSF}$. β_τ is the reliability index at τ time instant.

The time-dependent system failure probability P_{fsys} can be evaluated numerically as(Zhou et al., 2017):

$$P_{fsys}=1-\int_{-\infty}^{\beta_1}\cdots\int_{-\infty}^{\beta_n}\frac{1}{\sqrt{(2\pi)^n|\mathbf{R}_{LSF}|}}\times\exp\left(-\frac{1}{2}\boldsymbol{\theta}^T\mathbf{R}_{LSF}^{-1}\boldsymbol{\theta}\right)d\theta_1\cdots d\theta_n \tag{15}$$

For practical purpose, simple bounds on P_{fsys} can be given to avoid any numerical integration (J. Ji & Low, 2012; Madsen et al., 2006), the calculation of system failure probability in the next part used the method in (J. Ji & Low, 2012). In addition, (Gong & Zhou, 2017) presents an equivalent component approach for reliability analyses of series systems.

4. Rainfall-induced slope stability analysis

It is generally recognized that rainfall-induced landslides are caused by changes in pore water pressure and seepage force (Gerscovich et al., 2006). Furthermore, unsaturated soil slope failure is mainly due to the rainfall infiltration and loss in shear strength when soil suctions are decreased or dissipated (D.G Fredlund & Rahardjo, 1993). (Lumb, 1962) introduced the concept of wetting front in the investigation of slope failure under heavy rainfall in Hong Kong. Above the wetting front, the soil is assumed to be completely saturated, while the soil below the wetting front remains at the initial water content. Under the intensive rainfall condition (which means that the rainfall intensity is greater than the saturated soil permeability), there will be an obvious wetting front (**Fig. 1**) in the slope and the depth of the wetting front can be calculated as:

$$z_w=\frac{k_{sat}t}{n\left(S_f-S_0\right)} \tag{16}$$

where k_{sat} is the saturated coefficient of permeability, S_f is the final degree of saturation, S_0 is the initial degree of saturation, n is the porosity of the soil and t is the time. When taking the volumetric water content (VWC) into consideration, Eq (16) can be reformed as:

$$z_w=\frac{k_{sat}t}{\boldsymbol{\theta}_s-\boldsymbol{\theta}_0} \tag{17}$$

where θ_s is the saturated volumetric water content, θ_0 is the initial volumetric water content. The volumetric water content can be calculated by the soil-water characteristic curve (SWCC), which is the relationship between soil suction, ψ, and the volumetric water content, θ_w, and the unsaturated permeability function (ψ–k). The hydraulic conductivity and volumetric water content functions can be estimated using Fredlund and Xing's Model (Delwyn G Fredlund & Xing, 1994):

$$\boldsymbol{\theta}=\frac{\boldsymbol{\theta}_s}{\left\{\ln\left[e+\left(\frac{\boldsymbol{\psi}}{a}\right)^n\right]\right\}^m} \tag{18}$$

where *a, m, n* are the input parameters of the model, *e* is the natural logarithm, ψ is the suction of unsaturated soil.

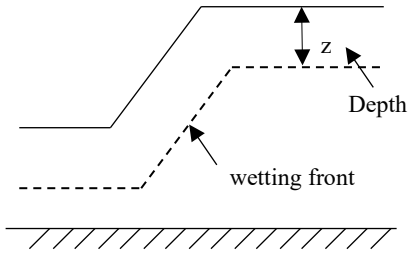

Figure 1. Lumb slope model

Based on the definitions of VWC and SWCC, the extended Mohr-Coulomb model can be used to estimate the shear strength of the slip surface. (Vanapalli et al., 1996) suggested a non-linear shear strength equation that involved a normalization of the volumetric water content function given by:

$$\boldsymbol{\tau}=c'+\left(\boldsymbol{\sigma}_n-\boldsymbol{\mu}_a\right)\tan\boldsymbol{\varphi}'+\left(\boldsymbol{\mu}_a-\boldsymbol{\mu}_w\right)\frac{\boldsymbol{\theta}-\boldsymbol{\theta}_r}{\boldsymbol{\theta}_s-\boldsymbol{\theta}_r}\tan\boldsymbol{\varphi}' \tag{19}$$

where τ is the shear strength, c' is the effective cohesion, (σ_n-u_a) is the net normal stress on the failure plane, σ_n is the total normal stress; u_a is the air pore-air pressure; u_w is the pore-water pressure; (u_a-u_w) is the matric suction; ϕ' is the friction angle; θ is the volumetric water content and the subscripts r and s indicate residual and saturation, respectively.

Since initial failures due to rainfall infiltration often have small depth-to-length ratios, the failure planes are parallel to the slope surface. Due to the infiltration of rainwater, the matrix suction at the wetting front is suddenly lost. Therefore, the most dangerous slip surface for rainfall-induced landslides is the wetting front plane (A.B.Fourie et al., 1999; DOU et al., 2016; Gavin & Xue, 2008; Muntohar & Liao, 2010). The use of infinite slope stability analysis for the evaluation of rainfall-induced landslides is justified and is often preferred for its simplicity(L. L. Zhang et al., 2011). Based on the infinite slope model (ISM) (**Fig. 2**), the factor of safety F_s can be expressed as follows:

$$F_s=\frac{\boldsymbol{\tau}_f}{\boldsymbol{\tau}_m} \tag{20}$$

where τ_f (kPa) is the shear strength of the potential sliding mass acting upon the slip surface, τ_m (kPa) is the gravity component of the potential sliding mass along the slipping direction.

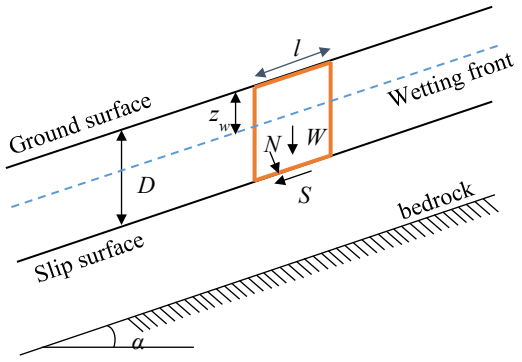

Figure 2. The infinite slope model and force conditions of the sliding mass element.

Referring to Fig. 2, the initial weight $W_{initial}$ of the potential sliding element (unit thickness) can be expressed as:

$$W_{\text{initial}}=\gamma D l\cos\alpha \tag{21}$$

where γ is the unit weight of soil, D is the depth of the potential sliding surface, l is the width of the potential sliding element, and α is the slope angle.
Due to rainfall, the soil above the wetting front becomes saturated from the initial condition. The soil water content increment is (θ_s-θ), so the weight increment of soil can be expressed as:

$$\Delta W=\gamma_w z_w l\cos\alpha(\theta_s-\theta) \tag{22}$$

where γ_w is the unit weight of water, z_w is the depth of the wetting front. The initial weight W_i of the potential sliding element (unit thickness) can be expressed as:

$$W=\left(\gamma D+\gamma_w z_w(\theta_s-\theta)\right)l\cos\alpha \tag{23}$$

The gliding force S and the normal force N can be expressed as:

$$S=W\sin\alpha=\left(\gamma D+\gamma_w z_w(\theta_s-\theta)\right)l\cos\alpha\sin\alpha \tag{24}$$

$$N=W\cos\alpha=\left(\gamma D+\gamma_w z_w(\theta_s-\theta)\right)l\cos^2\alpha \tag{25}$$

The corresponding stresses are:

$$\tau_m=\left(\gamma D+\gamma_w z_w(\theta_s-\theta)\right)\cos\alpha\sin\alpha \tag{26}$$

$$\sigma=\left(\gamma D+\gamma_w z_w(\theta_s-\theta)\right)\cos^2\alpha \tag{27}$$

Taking Eq (19), (26), (27) into Eq (20), the Fs can be calculated.

5. Case Study

An unsaturated soil slope with an inclination of 45° is selected for the next case study. Using the ISM model to calculate the slope stability in (WANG et al., 2016), and the instantaneous failure probability will be estimated by using the HLRF-x method.

The variables, which are independent, are summarized in Table 1, the initial soil suction is 50kpa and the SWCC parameters are shown as follows: θ_s=0.453, θ_r=0.148, a=7.21kpa, m=0.74, n=0.84.

Table 1. Statistical parameters of soil

Soil parameters	Distribution	Mean value	Standard deviation	Cross correlation
c'(kpa)	normal	8	3	$\rho_{c'\text{-}\varphi}$=0
φ'(°)	normal	38	4	$\rho_{c'\text{-}k_{sat}}$=0
k_{sat}(10^{-6}m/s)	lognormal	5	2.5	$\rho_{\varphi'\text{-}k_{sat}}$=0

Making a deterministic analysis to find the relationship between F_s and the rainfall duration (Fig. 3). It can be found that F_s decreases with the rising of rainfall duration, at around 42 hours, the slope is in critical failure state (F_s=1).

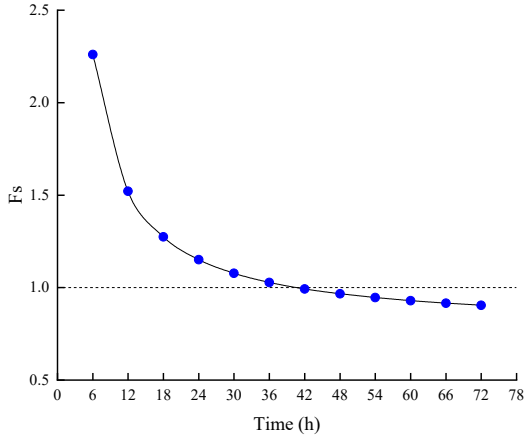

Figure 3. The relationship between Fs and rainfall duration

In order to calculate the reliability index automatically, a Python program was developed to compile the HLRF-x algorithm and the infinite slope model. The improved HLRF-x algorithm mentioned before is used to calculate the relationship between wetting front depth and reliability index. The reliability index at different time is shown in Fig. 4; it was found that the iteration numbers are less than ten when the difference between the calculation results of the two iterations is less than 0.001, which means that the improved HLRF-x method is effective to solve this problem.

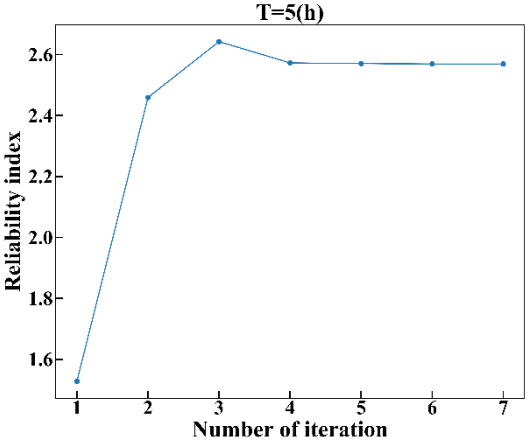

T=5h, reliability index=2.569

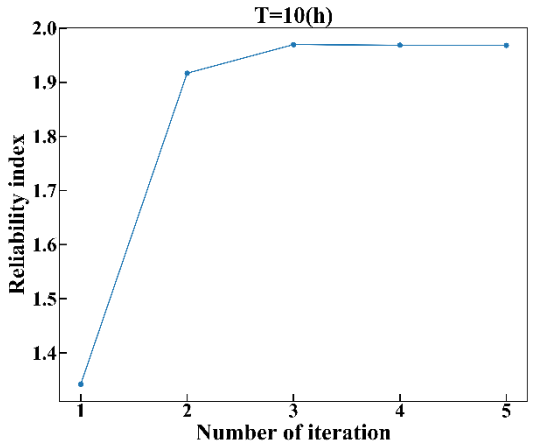

T=10h, reliability index=1.667

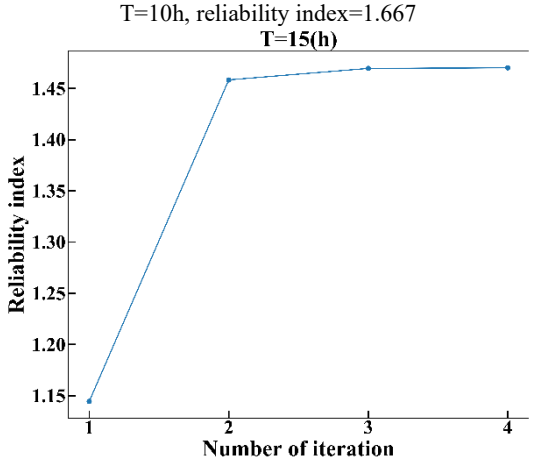

T=15h, reliability index=1.372

Figure 4. The reliability index at different time

The reliability index decreases during the rainfall process (Fig. 5), which means that the rainfall duration has an obvious influence on slope stability. At the time of 45 hours, the reliability index goes to the minimum value, which means the slope suffers a failure condition. When the rainfall duration is longer, the slope has more possibility to suffer an instability condition.

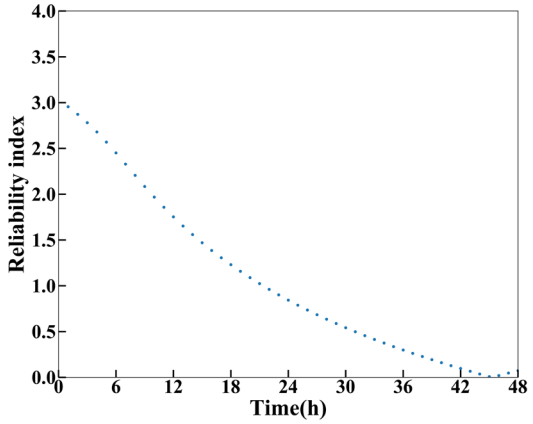

Figure 5. The instantaneous reliability index during the rainfall process

Using the system reliability analysis mentioned before, it can be found that the system failure probability converges when the interval number is 60~100 (Fig. 6), for this problem, we use 100 intervals to calculate the system failure probability. The system failure probability can be estimated by Eq (15) and two simple bounds in (J. Ji & Low, 2012; Madsen et al., 2006). Note that the bounds are very close because of the very high correlation between failure events at the discretized time instants, and the continuously decreasing reliability indices over time. The relation between the system failure probability and the duration of rainfall is shown in Fig. 7. At the initial 6 hours, the rainfall has little influence on the slope stability, the system failure probability is almost zero, then the system failure probability increases gradually in the rainfall duration. At the rainfall time of 45h, the system failure probability comes to about 0.5, the mean value goes into the failure domain. After 45h of rainfall, the slope is under instable condition. The trend of reliability analysis result is consistent with that of the slope safety factor changes, but the failure time of deterministic analysis is a little earlier than that of reliability analysis.

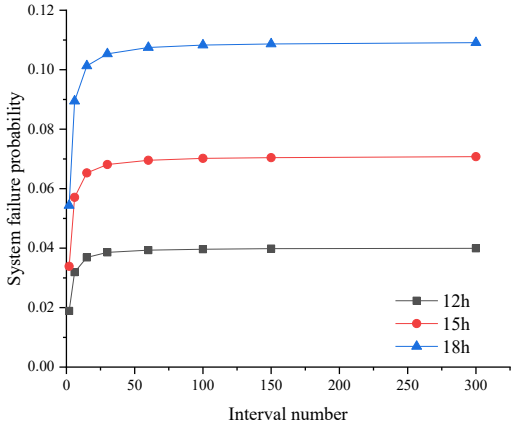

Figure 6. System failure probability VS. Intervals

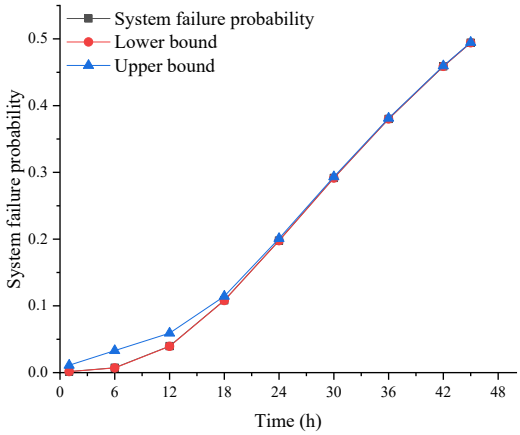

Figure 7. The system failure probability during the rainfall process

The probability sensitivity of each parameter to the slope system failure is defined as the degree of deviation from the mean value of soil parameters to the design point value. When the rainfall starts, the system failure probability begins to increase, the sensitivity of soil parameters is studied in Fig. 8, it can be found that both the cohesion and saturation permeability coefficient play

an important role on the slope stability at the beginning of rainfall. At the beginning of the rainfall (0~9h), the cohesion has the largest influence on the slope stability, followed by the saturation permeability coefficient. Then the influence of saturation permeability coefficient comes to largest during the middle rainfall duration (9~20h), in the end, the influence of cohesion increases to the largest. The change of friction angle is slight in the whole rainfall duration.

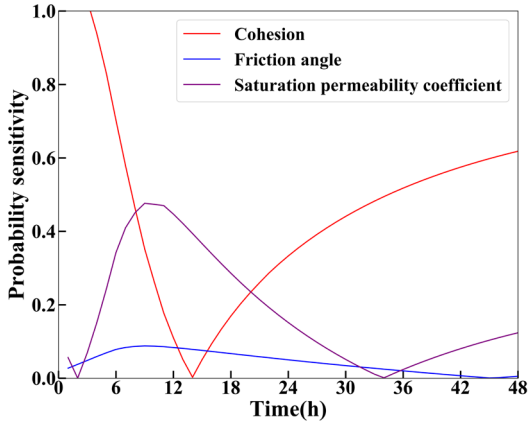

Figure 8. The probability sensitivity of uncertain soil parameters during rainfall

6. Conclusion

In this study, the HLRF-x algorithm for FORM analysis was used to calculate the time-dependent reliability of soil slope under intensive rainfall. For simplicity, the slope stability is influenced by the wetting front which is time-dependent. Then a series system reliability analysis method is used to solve the time-dependent reliability problem.

The Python platform is applied to realize the reliability analysis based on the ISM method.

From the case study, it was concluded that when suffering intensive rainfall, the failure probability of slope has an increasing trend and a landslide may occur. Both of the saturation permeability coefficient and cohesion of soil play important roles on the slope stability. The cohesion plays the most import role at the beginning of rainfall and at the former time of landslide occurs. The saturation coefficient of permeability may have the largest influence of slope failure during the mid-rainfall.

References

A.B.Fourie, D.Rowe, & G.E.Blight. (1999). The effect of infiltration on the stability of the slopes of a dry ash dump. *Geotechnique, Vol.49*(No.1), 1-13

Ang, A. H. S., & Tang, W. H. (1975). *Probability Concepts in Engineering Planning and Design*. New York: Wiley.

Baecher, G. B., & Christian, J. T. (2003). *Reliability and Statistics in Geotechnical Engineering*. NJ: Wiley.

DOU, H.-q., HAN, T.-c., GONG, X.-n., LI, Z.-n., & QIU, Z.-y. (2016). Reliability analysis of slope stability considering variability of soil saturated hydraulic conductivity under rainfall infiltration. *Rock and Soil Mechanics, 37*(4), 1144-1152

Fredlund, D. G., & Rahardjo, H. (1993). *Soil mechanics for unsaturated soils* : Wiley.

Fredlund, D. G., & Xing, A. (1994). Equations for the soil-water characteristic curve. *Canadian geotechnical journal, 31*(4), 521-532

Gavin, K., & Xue, J. F. (2008). A simple method to analyze infiltration into unsaturated soil slopes. *Computers and Geotechnics, 35*(2), 223-230.

Gerscovich, D. M. S., Jr., E. A. V., & Campos, T. M. P. d. (2006). On the evaluation of unsaturated flow in a natural slope in Rio de Janeiro, Brazil. *Engineering Geology, 88*(1-2), 23-40

Gong, C., & Frangopol, D. M. (2019). An efficient time-dependent reliability method. *Structural Safety, 81*.

Gong, C., & Zhou, W. (2017). Improvement of equivalent component approach for reliability analyses of series systems. *Structural Safety, 68*, 65-72.

Hasofer, A. M., & Lind, N. C. (1974). Exact and invariant second-moment code format. *Journal of the Engineering Mechanics division, 100*(1), 111-121

Ji, J., & Kodikara, J. K. (2015). Efficient reliability method for implicit limit state surface with correlated non-Gaussian variables. *International Journal for Numerical and Analytical Methods in Geomechanics, 39*(17), 1898-1911.

Ji, J., & Low, B. K. (2012). Stratified Response Surfaces for System Probabilistic Evaluation of Slopes. *Journal of Geotechnical and Geoenvironmental Engineering, 138*(11), 1398-1406.

Ji, J., Zhang, C., Gao, Y., & Kodikara, J. (2019). Reliability-based design for geotechnical engineering: An inverse FORM approach for practice. *Computers and Geotechnics*(111), 22-29

Li, C. D., Wu, J. J., Tang, H. M., Wang, J., Chen, F., & Liang, D. M. (2015). A novel optimal plane arrangement of stabilizing piles based on soil arching effect and stability limit for 3D colluvial landslides. *Engineering Geology, 195*, 236-247.

Liu, P.-L., & Der Kiureghian, A. (1991). Optimization algorithms for structural reliability. *Structural safety, 9*(3), 161-177

Low, B. K., & Tang, W. H. (2004). Reliability analysis using object-oriented constrained optimization. *Structural Safety, 26*(1), 69-89

Low, B. K., & Tang, W. H. (2007). Efficient spreadsheet algorithm for first-order reliability method. *Journal of Engineering Mechanics, 133*(12), 1378-1387.

Lumb, P. (1962). *Effect of rain storms on slope stability*. Proceedings of the Symposium on Hong Kong Soils, Hong Kong.

Madsen, H. O., Krenk, S., & Lind, N. C. (2006). *Methods of structural safety*. New York: Dover Publications, Inc.

Mahadevan, S., & Haldar, A. (2000). Probability, reliability and statistical method in engineering design. *John Wiley Sons*

Muntohar, A. S., & Liao, H.-J. (2010). Rainfall infiltration: infinite slope model for landslides triggering by rainstorm. *Natural Hazards, 54*(3), 967-984.

Rackwitz, R. (1976). Practical Probabilistic Approach to Design first Order Reliability Concepts for Design Codes. *Bulletin d'Information de CEB, 112*

Rackwitz, R., & Flessler, B. (1978). Structural reliability under combined random load sequences. *Computers and Structures, 9*(5), 489-494

Valdebenito, M. A., & Schuëller, G. I. (2010). A survey on approaches for reliability-based optimization. *Structural and Multidisciplinary Optimization, 42*(5), 645-663.

Vanapalli, S., Fredlund, D., Pufahl, D., & Clifton, A. (1996). Model for the prediction of shear strength with respect to soil suction. *Canadian geotechnical journal, 33*(3), 379-392

WANG, H., ZHANG, J., & CHEN, F. (2016). Time-depent reliability of slopes made of compeletely composed granite under intense rainfall. *Engineering Journal of Wuhan University, 49*(5), 763-767

Zhang, L. L., Zhang, J., Zhang, L. M., & Tang, W. H. (2011). Stability analysis of rainfall-induced slope failure: a review. *Proceedings of the Institution of Civil Engineers - Geotechnical Engineering, 164*(5), 299-316.

Zhang, Y., Tang, H., Li, C., Lu, G., Cai, Y., Zhang, J., & Tan, F. (2018). Design and Testing of a Flexible Inclinometer Probe for Model Tests of Landslide Deep Displacement Measurement. *Sensors (Basel), 18*(1), 224-.

Zhou, W., Gong, C., & Hong, H. P. (2017). New Perspective on Application of First-Order Reliability Method for Estimating System Reliability. *Journal of Engineering Mechanics, 143*(9).